This is the manuscript version of an article published in *Cardiovascular Research* (2023) 119, 1175–1189.
Version of record available at https://doi.org/10.1093/cvr/cvad009

Empagliflozin inhibits excessive autophagy through the AMPK/GSK3β signalling pathway in diabetic cardiomyopathy Purchased

Rosalinda Madonna[1], Stefania Moscato[2], Maria Concetta Cufaro[3,4], Damiana Pieragostino[4,5], Letizia Mattii[2], Piero Del Boccio[3,4], Sandra Ghelardoni[6], Riccardo Zucchi[6], Raffaele De Caterina[1]✉

[1] Cardiology Division, Department of Pathology, University of Pisa, Via Paradisa, 56124 Pisa, Italy

[2] Histology Division, Department of Clinical and Experimental Medicine, University of Pisa, Via Savi 10, 56126 Pisa, Italy

[3] Department of Pharmacy, 'G. d'Annunzio' University of Chieti-Pescara, Via Colle dell'Ara, 56100 Chieti, Italy

[4] Analytical Biochemistry and Proteomics Laboratory, Center for Advanced Studies and Technology (CAST), 'G. d'Annunzio' University of Chieti-Pescara, Via Colle dell'Ara, 56100 Chieti, Italy

[5] Department of Innovative Technologies in Medicine and Dentistry, 'G. d'Annunzio' University of Chieti-Pescara, Via Colle dell'Ara, 56100 Chieti, Italy

[6] Department of Pathology, Laboratory of Biochemistry, University of Pisa, Via Savi 10, 56126 Pisa, Italy

Abstract

Aims

Sodium-glucose cotransporter 2 inhibitors have beneficial effects on heart failure and cardiovascular mortality in diabetic and non-diabetic patients, with unclear mechanisms. Autophagy is a cardioprotective mechanism under acute stress conditions, but excessive autophagy accelerates myocardial cell death leading to autosis. We evaluated the protective role of empagliflozin (EMPA) against cardiac injury in murine diabetic cardiomyopathy.

Methods and results

Male mice, rendered diabetics by one single intraperitoneal injection of streptozotocin and treated with EMPA (30 mg/kg/day), had fewer apoptotic cells (4.9 ± 2.1 vs. 1 ± 0.5 TUNEL-positive cells %, $P < 0.05$), less senescence (10.1 ± 2 vs. 7.9 ± 1.2 β-gal positivity/tissue area, $P < 0.05$), fibrosis (0.2 ± 0.05 vs. 0.15 ± 0.06, $P < 0.05$ fibrotic area/tissue area), autophagy (7.9 ± 0.05 vs. 2.3 ± 0.6 fluorescence intensity/total area, $P < 0.01$), and connexin (Cx)-43 lateralization compared with diabetic mice. Proteomic analysis showed a down-regulation of the 5′ adenosine monophosphate-activated protein kinase (AMPK) pathway and upstream activation of sirtuins in the heart of diabetic mice treated with EMPA compared with diabetic mice. Because sirtuin activation leads to the modulation of cardiomyogenic transcription factors, we analysed the DNA binding activity to serum response elements (SRE) of serum response factor (SRF) by electromobility shift assay. Compared with diabetic mice [0.5 ± 0.01 densitometric units (DU)], non-diabetic mice treated with EMPA (2.2 ± 0.01 DU, $P < 0.01$) and diabetic mice treated with EMPA (2.0 ± 0.1 DU, $P < 0.01$) significantly increased SRF binding activity to SRE, paralleled by increased cardiac actin expression (4.1 ± 0.1 vs. 2.2 ± 0.01 target protein/β-actin ratio, $P < 0.01$). EMPA significantly reversed cardiac dysfunction on echocardiography in diabetic mice and inhibited excessive autophagy in high-glucose-treated cardiomyocytes by inhibiting the autophagy inducer glycogen synthase kinase 3 beta (GSK3β), leading to reactivation of cardiomyogenic transcription factors.

Conclusion

Taken together, our results describe a novel paradigm in which EMPA inhibits hyperactivation of autophagy through the AMPK/GSK3β signalling pathway in the context of diabetes.

1. Introduction

Diabetic cardiomyopathy, a condition characterized in its early stages by diastolic relaxation abnormalities and, later, by systolic dysfunction in the absence of dyslipidaemias, hypertension, coronary artery disease, and valvular heart disease, has an independent role in determining heart failure in diabetic patients.[1] Beyond the strict control of diabetes, there is a lack of valid therapeutic strategies to prevent its evolution towards heart failure, especially when the stigmata of diabetic cardiomyopathy and the consequent diastolic dysfunction have been established.

The pathogenesis of diabetic cardiomyopathy involves increased cardiomyocyte apoptosis and fibrosis, impaired cardiomyocyte autophagy and microangiopathy, often characterized by de-regulated angiogenesis and the formation of dysfunctional small vessels.[2,3] Cellular autophagy or autophagocytosis is the self-cannibalization mechanism of cells with which the selective removal of damaged cytoplasmic components takes place. Autophagy is involved in maintaining cardiac function; however, autophagy is hyperactivated in pathological conditions, including heart failure,[4] cardiac hypertrophy,[5] ischaemic cardiomyopathy,[6] and cardiac senescence.[7] Especially in the pathogenesis of diabetic cardiomyopathy, excessive and de-regulated autophagy appears to play a

key role.[8,9] Therefore, autophagy can represent a valid target for limiting damage in diabetic cardiomyopathy.

Several trials have shown beneficial effects of empagliflozin (EMPA), a selective inhibitor of the sodium-glucose cotransporter 2 (SGLT2), on heart function and cardiovascular outcomes in diabetic patients with Type 2 [10,11] and Type 1 diabetes,[12,13] although the underlying mechanisms are unknown. In this work, we aimed at examining the protective role of EMPA against cardiac injury in a murine model of diabetic cardiomyopathy and assessed underlying mechanisms, hypothesizing that EMPA can target excessive autophagy and adverse cardiac remodelling, thus explaining the prevention of heart failure in diabetic cardiomyopathy.

2. Methods

EMPA was purchased from Santa Cruz Biotechnology (Santa Cruz, CA, USA). Unless otherwise specified, all other reagents were from Sigma-Aldrich (St. Louis, MO, USA).

2.1 Animal care and experimental procedures

Male C57BL/6 mice (body weight: 30 ± 4 g, 6 months old) were purchased from Charles River Italia. Treatment with STZ, to make the mice diabetic, and with EMPA were carried out as previously described (see Supplementary material online, Figure S1).14 Briefly, mice were provided with ad libitum rodent chow (Teklad 7001, 4.4%; Harlan Teklad Global Diets) and water. Mice were randomized into four groups (n = 8 for each treatment group): vehicle (saline) or CNTRL, EMPA, STZ, STZ + EMPA. Type 1 diabetes mellitus (T1DM) was induced by one single intraperitoneal injection of streptozotocin at 30 mg/kg dissolved in 0.01 mol/L citrate buffer (pH 4.5). With this diabetes induction protocol, the mortality of mice was zero. EMPA was dissolved in water and administered to mice in the experimental groups after 1 month from Type 1 diabetes induction, by oral gavage daily (30 mg/kg/day for 28 days, corresponding to the equivalent active dose in humans; https://go.drugbank.com/drugs/DB09038). For echocardiograms, mice were anesthetized by intraperitoneal injection of ketamine (100 mg/kg, Clorketam; Vétoquinol, Italy), according to procedures already described.[14] At 1 month from EMPA treatments, the animals were anesthetized by inhalation of 2–5% isoflurane in oxygen and sacrificed via cervical dislocation. The hearts were excised, snap-frozen in liquid nitrogen, and stored at −80°C for protein extraction or embedded in optical cutting temperature (OCT) medium for histological analyses. All procedures were approved by the local Institutional Ethics Committee for Animal Research (Protocol number 176/2019-R released on 25 February 2019). All studies conformed to the Guidelines from Directive 2010/63 EU of the European Parliament on the protection of animals used for scientific purposes of the National Institutes of Health guidelines.

2.2 Blood chemistry analyses

Blood was collected from the tail veins of diabetic and non-diabetic mice. Blood glucose and insulin levels were measured using a glucometer (GR-102, Terumo, Tokyo, Japan) or by ELISA Kit (AKRIN-011T, Shibayagi, Gunma, Japan), respectively.

2.3 Image analysis

All sample sections were observed under the BX43 microscope (EVIDENT Europe GmbH, Hamburg, Germany) and captured by an SC50 digital camera (EVIDENT Europe; pixel dimension photo camera sensor 2.2 × 2.2 μm, LED light), as described in the Supplementary material online.

2.4 Cell cultures

H9c2 cells[15–17] purchased from American Type Culture Collection (ATCC, Rockville, MD, USA) were cultured in high glucose Dulbecco's modified Eagle's medium (DMEM, ATCC) supplemented with 10% heat-inactivated foetal bovine serum (FBS) under 95% air and 5% CO_2 at 37°C. Differentiation into cardiomyocytes was performed as previously described.[18] In brief, cells were cultured in DMEM containing 1% FBS and all-trans retinoic acid supplementation (50 nM) for 10 days. At subconfluence (70–80%), cardiomyocytes cultured in Petri dishes [for electrophoretic mobility shift assays (EMSA) and immunoblotting] or chamber slides (for autophagy assay) were preincubated for 30 min with EMPA (100 and 500 nM) or wortmannin (100 nM), followed by the addition of D-glucose (30 mM) for 24 h.

2.5 Fibrosis analysis

The hearts in OCT were cut transversely to obtain 10 μm thick sections from the middle of the ventricles. Morphology and interstitial, perivascular, and coronary arterial fibrosis were assessed by haematoxylin–eosin and picrosirius red staining, respectively. The extent of left ventricular (LV) fibrosis was quantified by image analysis.

2.6 Terminal deoxyribonucleotidyl transferase-mediated dUTP nick end labelling assay

Detection of nuclei with fragmented DNA was performed using the HRP-DAB terminal deoxyribonucleotidyl transferase-mediated dUTP nick end labelling (TUNEL) assay kit (Abcam, Cambridge, UK) according to the manufacturer's instructions and as previously described.[14] The myocardial apoptotic index was calculated as the mean percentage of TUNEL-positive cells on a total cell number ranging between 600 and 2000. The TUNEL assay was read under a standard light microscope by two blinded, independent researchers.

2.7 Senescence-associated β-galactosidase assay

Cardiac senescence was evaluated by senescence-associated-β-galactosidase staining (SA-β-gal Activity) (Cell Biolabs, Inc., San Diego, CA, USA), as previously described.[14] The senescence assay was read under a standard light microscope and the extent of the blue-stained area was evaluated by image analysis.

2.8 Autophagy detection by immunofluorescence

Autophagy in murine heart sections and cardiomyocytes plated in chamber slides were detected by Autophagy Detection Kit (Abcam ab139484, Cambridge, UK), as previously described.[19] Briefly, cardiac sections or chamber slides with cardiomyocytes were incubated with fluorescent dyes for nuclei staining and autophagy detection. After washing, the green fluorescence was observed under a confocal microscope (Carl Zeiss LSM 510 META Laser Confocal Microscope, Oberkochen,

Germany) and quantified by image analysis. The Green Detection Reagent was read with a fluorescein isothiocyanate filter (Excitation ~480 nm, Emission ~530), and the Hoechst 33342 Nuclear Stain was read with a 4',6-diamidino-2-phenylindole filter set (340/480 ex/em).

2.9 Immunohistological evaluation of capillary and arterioles density

We examined the effects of STZ and EMPA on the capillaries and arterioles density by immunohistochemical analyses for CD31, alpha-smooth muscle actin (ASMA), and vascular endothelial (VE) cadherin in OCT-embedded cardiac tissue sections, as previously described[20] and stated in the Supplementary material online. The ASMA and VE-cadherin immunofluorescence staining was assessed under a fluorescence microscope at excitation ~598 nm and emission ~625. The CD31 immunoperoxidase staining was read under a standard light microscope. The immunopositivities (immunoperoxidase and immunofluorescence) were quantified by image analysis.

Moreover, vessel density was evaluated at ×400 total magnification by two blinded, independent observers on 10–20 fields, in order to cover the whole section, and it was expressed as the percentage of the vessel number by tissue area.

2.10 Immunohistochemical evaluation of connexin protein expression

Expressions of Cx43, pS368-Cx43, and Cx26 were evaluated by immunofluorescence analysis cadherin in OCT-embedded cardiac tissue sections, as previously described[20] and stated in the Supplementary material online. The connexins immunofluorescence staining was assessed under a fluorescence microscope at excitation ~598 nm and emission ~625, and quantified by image analysis.

2.11 Proteomics and computational analyses

Cardiac tissue from each treatment group was digested following the Filter Aided Sample Preparation method and label-free shotgun proteomics experiments were carried out as previously described.[19,21] The mass spectrometry proteomics data have been deposited to the ProteomeXchange Consortium via the PRIDE partner repository.

A panel of differential proteins (considering only unique proteins) was subjected to an in silico analysis by the Ingenuity Pathway Analysis (Ingenuity Systems, Mountain View, CA, USA) and Gene Ontology. Results were visualized as principal component analysis and volcano plots (see Supplementary material online, Figures S2 and S3).

2.12 Immunoblotting

Total proteins were isolated from the hearts in an ice-cold RadioImmuno Precipitation Assay, separated under reducing conditions, and electroblotted onto polyvinylidene fluoride membrane (Immobilon-P, Millipore, Bedford, MA, USA), as previously described [18,20,21] and detailed in the Supplementary material online. The expression of each target was provided as the ratio between the densitometry of the target protein and the densitometry of the 'housekeeping' protein control (GAPDH or β-actin).

2.13 Electrophoretic mobility shift assays

Nuclear fractions and EMSA were performed using a non-radioactive Chemiluminescent EMSA Kit (Signosis Inc., Santa Clara, CA, USA), as described in the Supplementary material online.

2.14 Serum response factor cell-based phosphorylation assay

Cardiomyocytes were seeded in 96-well plates at 30 000 cells/well overnight in high glucose DMEM medium. The following day, the cells were serum-starved (2% fetal calf serum) for 6 h, preincubated for 30 min with 500 nM EMPA, followed by the addition of D-glucose (30 mM) for 24 h. After treatment, plates were used to assess serum response factor (SRF) phosphorylation using a phosphospecific antibody cell-based ELISA kit (LSBio, Seattle, WA, USA), as described in the Supplementary material online. Results were expressed as a ration between pSRF normalized for cell nuclei/SRF normalized for cell nuclei or GAPDH normalized for cell nuclei.

2.15 Echocardiography

We performed transthoracic echocardiography blindly at 1 month after treatments using a portable ultrasound apparatus (Esaote, Genoa, Italy, for pulse wave doppler analyses; Vevo 770 system, Visualsonics, the Netherlands, for M- and B-mode analyses) equipped with a 40 MHz linear probe according to detailed protocols previously described.[14] Specifically, investigators who analysed the images were blinded to treatment groups.

2.16 Statistical analysis

Data are expressed as mean ± standard deviation. Multiple-group comparisons were performed by analysis of variance (ANOVA) and the Tukey Honestly Significant Difference (HSD) post hoc test P and, where necessary, Student's t-test. Values <0.05 were considered statistically significant. SPSS and GraphPad software were used for data processing and statistical analysis.

3. Results

3.1 Functional and structural profiles of hearts from diabetic mice and controls treated with empagliflozin

Diabetic mice were lean, with higher plasma glucose levels and lower insulin levels, compared with non-diabetic control mice (see Supplementary material online, Table S1). At echocardiography, systolic (Figure1A and B) and diastolic (Figure 1C) cardiac functions were significantly impaired in diabetic mice, with an increase in LV diameter (Figure1D and E). Haematoxylin–eosin staining did not evidence relevant morphological differences among treatments (Figure 2A). Pathological examination revealed more cardiac fibrosis in parallel with changes in diastolic cardiac function (Figure2B and C). EMPA treatment attenuated systolic (Figure1A and B) and diastolic dysfunction (Figure 1C), cardiac fibrosis (Figure2B and C), and the expression of type III collagen (Figure 3B). In the ventricles of STZ-treated mice, the total number of TUNEL-positive apoptotic cells was four-fold higher than in vehicle-treated controls (Figure2D and F). These effects were reversed by co-treatment with EMPA. In the ventricular myocardium of STZ-treated mice, the percentage of SA β-gal-positive senescent cardiac area was 2.5-fold higher than in vehicle-treated controls (Figure2E

and G). At immunoblotting, there was a significant increase in the expression of a more sensitive marker of senescence p16INK4A expression in the hearts of STZ-treated mice compared with vehicle-treated controls (Figure 2H). EMPA reversed the effect of STZ on cardiac apoptosis (Figure2D and F) and showed a trend of reduction in senescence (Figure 2E, G, and H). Whereas there was a significant decrease in p16INK4A expression (Figure 2H), and a trend of reduction in fibrosis and in the number of apoptotic cells after EMPA treatment in non-diabetic control mice, EMPA induced no significant changes in collagen deposition, cardiac apoptosis, and senescence in the absence of diabetes (Figures 2A–H and 3B). The effects of EMPA on cardiac apoptosis were also supported by label-free proteomics analysis in the hearts of diabetic mice. As shown in Supplementary material online, Figure S4A–C, compared with STZ-treated hearts, protein cargo of STZ + EMPA-treated hearts was able to inhibit cellular functions related to 'necrosis' [−Log(P-value) = 9.26, z-score = −2.3], 'apoptosis of muscle cells' [−Log(P-value) = 9.11, z-score = −2.3], and 'cell death of cardiomyocytes' [−Log(P-value) = 8.66, z-score = −2.3].

3.2 Empagliflozin exerts an anti-lymphangiogenesis effect in diabetic mice independent of the vascular endothelial growth factor signalling pathway

Cardiac remodelling in diabetic hearts includes not only fibroblast activation and fibrosis, but also increased angiogenic and lymphangiogenic response.[22] Therefore, we evaluated the impact of EMPA on angiogenesis and lymphangiogenesis, and the expression of angiogenic markers. Compared with STZ-treated mice, STZ + EMPA had lower CD31-positive vessel density and CD31 reactivity degree with no statistically significant differences in VE-cadherin-positive vessel density as well as VE-cadherin and ASMA reactivity degree (Figure 3A). These data could represent an EMPA effect on lymphatic vessels only. Indeed, immunopositivity for the blood vessel marker VE-cadherin did not change after EMPA administration. However, the decrease of the lymphatic vessels by EMPA is consistent with the results obtained on fibrosis and indicates an anti-remodelling effect exerted by EMPA. Activation of several angiogenic growth factor receptors [vascular endothelial growth factor receptor-1 (VEGFR-1 or Flt1), fibroblast growth factor receptor, platelet-derived growth factor receptor[23]], matrix metalloproteinases,[24] and aquaporin water channel (AQP)-1 are all involved in the angiogenic and lymphangiogenic process.[25,26] In the present study, we evaluated cardiac collagen III and VEGFA protein expression. Compared with STZ-treated mice, STZ + EMPA had lower collagen III expression and higher VEGFA expression. Therefore, the irrelevance of EMPA on the blood and lymphatic vessel density was not paralleled by an equal effect on VEGFA expression (Figure 3C) and signalling pathway (see Supplementary material online, Figure S4F and G), suggesting that EMPA acts on lymphangiogenesis independently of the VEGFA signalling pathway.

3.3 Empagliflozin attenuates autophagy in diabetic hearts

Because insulin inhibits autophagy, we hypothesized that autophagy would be increased in STZ-induced diabetes, reflecting insulin deficiency. Abundant green fluorescent protein positivity was observed in the hearts of diabetic mice (Figure 4A). Western blot analysis showed expression of SGLT2 in murine hearts, with substantial variability depending on the type of treatment, with the highest expression in the hearts of diabetic mice and the lowest expression in non-diabetic mice exposed to EMPA (Figure 4B). The specificity of the anti-SGLT2 antibody was verified by using the blocking peptide (BP) in the heart protein samples treated with STZ (STZ + BP), in which the

blocking peptide was able to significantly reduce the binding of the antibody to the target protein SGLT2 (Figure 4B). Using immunoblotting we found that the expression of microtubule-associated protein 1 light chain 3 (LC3)-II was up-regulated in diabetic mice (Figure 4C), as it was for the expression of p62 (SQSTM1/sequestrome 1), a selective substrate of autophagy (Figure 4D). These effects were reversed by co-treatment with EMPA, suggesting that EMPA acts on cardiac autophagy (Figure4C and D). We observed a significant increase in the level of activated 5' adenosine monophosphate-activated protein kinase (phosphorylated AMPK; p-AMPK) in STZ-treated diabetic hearts, which was reversed by co-treatment with EMPA (Figure 4F). There was a significant decrease in p-AMPK expression after EMPA treatment in non-diabetic control mice (Figure 4F). The effects of STZ and EMPA on AMPK were also supported by label-free proteomics analysis. As shown in Supplementary material online, Figure S5A and B compared with STZ-treated hearts, protein cargo of STZ + EMPA-treated hearts was able to inhibit the AMPK signalling pathway [−Log(P-value) = 3.02, z-score = −2.44]. These effects of EMPA were also paralleled in the hearts of non-diabetic control mice [−Log(P-value) = 1.98, z-score = −3.23]. Overall, these results indicate the presence of enhanced autophagy in the hearts of diabetic mice and the effect of relieving excessive STZ-induced autophagy by EMPA. Unexpectedly, the expression of active mTOR (p-mTOR) was increased in EMPA-treated STZ diabetic hearts (Figure 4E). Indeed, the insulin suppression that characterizes Type 1 diabetes should be accompanied by a reduction in p-mTOR.[27] Autophagy in the present setting thus appears not to be dependent on mTOR activity, probably due to the model used in this study, which is closer to a mixture of Type 1 and Type 2 diabetes.

3.4 Empagliflozin induces SIRT1 and SIRT3 and activates promyogenic transcription factors in diabetic and control hearts

Sirtuins could both activate and inhibit autophagy by activating several downstream signal pathways.[28] Among the seven sirtuins identified, SIRT1 is mainly located in the nucleus and SIRT3 is often in the mitochondrion, and both are targets of EMPA in cardiac tissue.[29,30] Therefore, we evaluated the impact of EMPA and STZ on the expression of SIRT1 and SIRT3. Compared with STZ-treated mice, STZ + EMPA showed a significant increase in SIRT1 and SIRT3 expression with no statistically significant differences in SIRT1 expression in STZ-treated vs. vehicle-treated mice (Figure 5A). These effects of EMPA on SIRT1 and SIRT3 were also paralleled in the hearts of non-diabetic control mice. The effects of STZ and EMPA on sirtuins were also supported by label-free proteomics analysis. As shown in Supplementary material online, Figure S6, compared with vehicle-treated hearts, protein cargo of EMPA-treated hearts was able to activate SIRT3 [−Log(P-value) = 4.22, z-score = 2.0] (Panel A) and sirtuin pathway [−Log(P-value) = 54.1, z-score = 2.94] (Panel B), whereas STZ was able to inhibit sirtuin pathway [−Log(P-value) = 53.9, z-score = −4.52] (Panel C). Because sirtuins interact with SRF[31] and myocardin-related transcription factor,[32,33] and sirtuin activation leads to modulation of cardiomyogenic transcription factors,[31–33] we analysed the DNA binding activity of SRF by electromobility shift assay, as well as the expression of myogenic transcription factors and sarcomeric proteins that are regulated by serum response element (SRE)/SRF binding activity. EMPA and STZ + EMPA significantly increased SRF/SRE binding activity compared with vehicle and STZ alone (Figure 5B), which was paralleled by increased cardiac actin expression in STZ + EMPA samples compared with STZ ones (Figure 5C). We did not observe any modulation of total or nuclear expression of SRF and myocardin in any treatment

group (data not shown). EMPA induced a significant increase in MTRF expression in both non-diabetic and diabetic mice (Figure 5C).

3.5 Empagliflozin inhibits autophagy through GSK3β in cardiomyocytes chronically exposed to high glucose

Glycogen synthase kinase 3 beta (GSK3β) in its active state, i.e. when it is dephosphorylated in serine 9 (Ser^{9}), induces autophagy via wortmannin-induced inhibition of the PI3K-Akt pathway.[34] In its active state, GSK3β phosphorylates SRF at the specific phosphorylation motif [(T/SPPXS): SPDSPPRSDPT, located in a highly conserved sequence of SRF], inducing its degradation.[34] Phosphorylation of serine 473 (Ser^{473}) is required for maximal activation of AKT.[35] We hypothesized that EMPA could inhibit excessive autophagy in the hearts of STZ-treated mice via the GSK3β/PI3K-Akt signalling pathway, leading to reactivation of the cardiomyogenic transcriptional complex. First, we verified the phosphorylation status of GSK3β and AKT in diabetic hearts and controls exposed to EMPA (Figure 5D). Diabetic hearts showed significantly lower levels of Ser^{9}-pGSK3β and Ser^{473}-pAKT compared with controls, suggesting a mutually opposite effect of activation and deactivation played by Type 1 diabetes on GSK and AKT, respectively. EMPA reversed the effect of STZ on Ser^{9}-pGSK3β and Ser^{473}-pAKT. These effects of EMPA on Ser^{473}-pAKT but not Ser^{9}-pGSK3β were also paralleled in the hearts of non-diabetic control mice (Figure 5D). We next expanded the in vivo studies by investigating whether GSK3β/PI3-AKT conveys the autophagy demodulation signal of EMPA in cardiomyocytes chronically exposed to high glucose levels. We used rat cardiomyocytes derived from differentiating H9C2 cells and cultured in DMEM high glucose. We demonstrated expression of SGLT2 in these cells at western blot, albeit with substantial variability depending on the treatment type, with the highest expression in those that received an acute addition of 30 mM glucose to the culture medium for 24 h (Figure 6A). Consistent with in vivo experiments, cardiomyocytes treated with 500 nM EMPA showed significantly higher levels of Ser^{9}-pGSK3β and Ser^{473}-pAKT than basal conditions (CNTRL), and an acute addition of 30 mM glucose for 24 h to the culture medium or wortmannin treatment further reduced them (Figure 6A). EMPA reversed the effects of 30 mM glucose with or without wortmannin on Ser^{9}-pGSK3β but not on Ser^{473}-pAKT (Figure 6A). We verified consistent activation of autophagy under basal conditions, at levels comparable with those induced by rapamycin (positive control) (Figure6B and C). Inhibition of GSK3β and AKT phosphorylation by wortmannin further increased autophagy (Figure 6B). The addition of 30 mM glucose in the culture medium did not further increase autophagy, whereas exposure to 500 nM EMPA in the presence or absence of wortmannin reduced autophagy back to levels below basal conditions (CNTRL), rapamycin and especially wortmannin (Figure 6B). Taken together, the data on GSK3β and AKT phosphorylation and autophagy suggest a specific action of EMPA on the GSK3β pathway to shut down excessive autophagy.

3.6 Empagliflozin reactivates the cardiomyogenic SRF–SRE transcriptional complex in cardiomyocytes chronically exposed to high glucose

SRF binds to SRE of DNA sequences located in the promoter of genes critical for cardiovascular myogenesis.[36] The stability of SRF is a requirement for the formation of the SRF–SRE complex. The ubiquitin–proteasome system[37] and the autophagy-dependent pathway[34] represent the main systems that regulate the stability and degradation of SRF and, therefore, its interaction with SRE.

In particular, activation of GSK3β has been shown to lead to phosphorylation and subsequent degradation of SRF through regulation of autophagy.[34]

First, we verified the phosphorylation status of SRF in cardiomyocytes chronically exposed to high glucose levels (Figure 6C). Cardiomyocytes treated with 500 nM EMPA showed levels of Ser^{9}-pSRF comparable with basal conditions (CNTRL), and acute addition of 30 mM glucose for 24 h to the culture medium significantly increased them when compared with basal condition (CNTRL) (Figure 6C). EMPA reversed the effects of 30 mM glucose on Ser^{9}-pSRF (Figure 6C). To determine if the shutdown of excessive autophagy operated by EMPA through GSK3β signalling pathway leads to effects on SRF–SRE interaction and contractile protein expression, we performed EMSA with nuclear extracts from cardiomyocytes chronically exposed to high glucose incubated with a non-radiolabelled double-stranded DNA SRE probe. In nuclear protein extracts from cells chronically treated with high glucose, a slight binding activity was indicated by the appearance of slightly shifted bands (Figure 6D). The specificity of SRF–SRE binding was confirmed by competition with unlabelled (cold) probe, which led to the disappearance of shifted bands. Cells treated with 500 nM EMPA showed significantly higher levels of SRF–SRE complex compared with basal conditions (CNTRL), and acute addition of 30 mM glucose for 24 h to the culture medium or treatment with wortmannin further reduced it, suggesting the presence of an inhibitory brake on SRF–SRE interaction exerted by exposure to high glucose and inhibition of GSK/PI3-AKT signalling pathway (Figure 6D). EMPA reversed the effects of 30 mM glucose with and without wortmannin on SRF–SRE binding (Figure 6D), suggesting the drug's ability to reactivate SRF–SRE binding activity inhibited by high glucose and GSK3β/PI3-AKT pathway inhibition.

3.7 Empagliflozin attenuates Cx43 lateralization distribution in diabetic mice and modulates Cx expression/activation in non-diabetic mice

Connexins (Cxs) are membrane-spanning proteins that play an essential role in cardiac function and disease[38] including diabetes cardiomyopathy,[39,40] through their canonical role in the propagation of electrical activity throughout the heart and their non-canonical role in the modulation of different cellular activities, including autophagy.[40,41] Therefore, we evaluated the expression of Cx43, the most studied Cx, and Cx26, the most recently found Cx in cardiomyocytes[18] and in whole heart tissues. The results obtained from both the western blot and the immunofluorescence showed that Cx43 expression did not change neither in STZ nor in EMPA-treated diabetic mice. Of note, non-diabetic mice treated with EMPA showed a significant reduction of Cx43 expression in total cardiac tissue lysates which was paralleled by a corresponding decrease of its expression in cardiomyocytes, as revealed by immunofluorescence analysis (Figure7A and B). In this model, we also evaluated the expression of the phosphorylated form of Cx43 at serine 368 (pS368-Cx43) which is involved in the specific permeability of Cx43-made junctions.[38] Similarly to Cx43 expression, pS368-Cx43 did not vary in STZ and EMPA-treated diabetic mice compared with control as a result of both western blot and immunofluorescence analysis. Conversely, pS368-Cx43 expression increased with EMPA administration in non-diabetic mice (Figure7A and B). Moreover, we also investigated Cx43 distribution in cardiomyocytes. Indeed, Cx43 is usually localized at intercalated discs while a lateral distribution has been observed in different heart diseases.[38] We quantified the Cx43 lateralization by excluding the tissue area where Cx43 and N-cadherin were co-localized, as shown in Figure 7C. We found that lateralization of Cx43 observed in STZ-treated mice was significantly reduced by EMPA treatment. Regarding

Cx26 expression, we observed that this Cx was significantly reduced in the total heart tissue lysates harvested from STZ-treated mice, and EMPA treatment tended to revert this effect even without a statistically significant difference (Figure 7D). In contrast, in cardiomyocytes of normal mice, EMPA administration induced a decrease in the Cx26 expression as shown by immunofluorescence results (Figure 7D).

4. Discussion

In the present study, we demonstrated that empagliflozin (EMPA) attenuated LV dysfunction, remodelling, fibrosis, lymphangiogenesis, and myocyte apoptosis in a murine model of diabetic cardiomyopathy. In this model, hyperactivation of autophagy was apparently involved in the pathogenesis of diabetic cardiomyopathy and EMPA appears to exert its cardiac protective action against hyperglycaemia-induced deterioration, at least in part, through the inhibition of excessive autophagy triggered by hyperglycaemia. This process is mediated through the inactivation of the GSK3β pathway, rather than through the AKT pathway, and this resulted in increased interaction of SRF with SRE and subsequent up-regulation of cardiac actin expression (Figure 8).

In this study, we also explored a possible Cx involvement in the cardiac protective pathway triggered by EMPA. Cardiac Cxs are proteins responsible for proper cardiac function. They form gap junctions that mediate electrical signalling and allow for synchronized contraction. Moreover, they can take part in several transduction pathways, interacting individually with intracellular signal molecules. In the present study, the protective EMPA pathway seems to involve Cx43 given that the use of EMPA on diabetic mice induced a decrease in lateral Cx43. The lateralization of Cx43 in cardiomyocytes consists in the displacement of Cx from the region of sarcolemma containing the intercalated discs, which allows the electrical and physical coupling between adjacent cardiomyocytes, to the lateral membrane, which allows the interaction between cardiomyocytes and the extracellular matrix. An increase in Cx43 lateralization along with or without a decrease in Cx43 expression is often associated with cardiac alterations as has also been demonstrated in some rat models of diabetes.[38] Even though our diabetic model did not have these Cx43 changes (probably due to the characteristics of the different models), the significant reduction of Cx43 lateralization induced by EMPA in diabetic mice could represent its protective action that was partly reflected in the attenuation of ventricular dysfunction. Indeed, as the Cx43 expression of cardiomyocytes did not change in diabetic mice after EMPA administration, a decrease in Cx43 lateralization could correspond to an increase of Cx43 at intercalated discs to form gap junctions. This increase of Cx43 at the intercalated discs is considered protective of cardiac dysfunctions by improving the electrical signal.[38] In the present study, Cx26 did not appear to be involved in the protective pathway induced by EMPA. However, its expression decreased in the heart tissue of diabetic mice, namely in cells other than cardiomyocytes. Indeed, the decrease in Cx26 was observed in cardiac lysate samples from diabetic mice by western blotting but not in cardiomyocytes by immunofluorescence. Cx26 represents the most recent Cx found in cardiomyocytes. It is expressed at the level of several cytoplasmic organelles but not at the level of intercalated discs and although its involvement in a gap junction-independent, intra- and inter-cellular communication has been suggested, its function is not yet clear.[18,42] It is noteworthy the EMPA's action on cardiac Cx expression of non-diabetic mice. Specifically, EMPA induced a

significant decrease in Cx43 and Cx26 in cardiomyocytes of non-diabetic mice. This decrease could justify the increase in autophagy observed in the present study. Indeed, a negative regulatory role in autophagic flux has been demonstrated for Cx43, Cx32, and Cx26 as well as the independence of this role from the gap junction function.[41] Cxs might suppress autophagy probably by recruiting plasma-membrane autophagy-related proteins, as stated for Cx43 in mouse osteoblast cells.[43] Due to the scarce literature on cardiac Cx26, these results are important as they demonstrate modulation of cardiac Cx26 expression in response to experimental diabetes or drugs, like EMPA. Finally, EMPA increased pS368-Cx43 in non-diabetic mice. In general, a reduced expression of Cx43 and an increase in its phosphorylated form, pS368-Cx43, are associated with cardioprotection.[38]

Autophagy is an important mechanism of organ homoeostasis maintenance.[44,45] However, the role of autophagy in pathological conditions, particularly in diabetic cardiomyopathy, is still controversial. Diabetic cardiomyopathy is associated with either down-regulation[46–48] or hyperactivation of autophagy in diabetic mice.[49,50] The controversial results are highly dependent on the type of diabetes, whereby autophagy is down-regulated in the hearts of Type 2 diabetic mice, whereas it is up-regulated in the hearts of Type 1 diabetic mice.[51] In different settings such as ischaemic heart disease, autophagy plays a protective role during ischaemia but is detrimental during reperfusion.[27]

Autophagy also occurs in the failing human heart, and up-regulation has been reported in animal models of pressure overload-induced heart failure, where autophagy may antagonize ventricular hypertrophy by increasing protein degradation.[52] In contrast, in load-induced heart failure, the extent of autophagic flux can rise to maladaptive levels. Excessive autophagy induction leads to autophagic cell death and loss of cardiomyocytes and may contribute to the worsening of heart failure.[52] Accordingly, the relevance of empagliflozin as a therapy for heart failure that down-regulates the cell death aspects of autophagy would be of great value in the treatment of patients with load-induced heart failure, as well as in patients with diabetic cardiomyopathy.

In the present study, we used a mouse model of Type 1 diabetes induced by a single intraperitoneal injection of STZ, and a short course of diabetes (over 1 month) induced mild LV dilation, mild systolic and diastolic dysfunction, a condition that mimics early human diabetic cardiomyopathy. We observed overactive autophagy in the myocardium of diabetic mice and in cardiomyocytes cultured in high glucose. Thus, overactive autophagy plays a key role in the pathogenesis of diabetic cardiomyopathy.

An important finding of the present study was that empagliflozin attenuated diabetic cardiomyopathy via down-regulation of GSK3β-mediated autophagy. Indeed, our in vitro data demonstrated that empagliflozin in turn promoted GSK3β inactivation through its phosphorylation and activated nuclear translocation of SRF and its interaction with SRE, which was suppressed by hyperglycaemia in the diabetic mouse model and high glucose in cardiomyocytes.[53] Here, high glucose-induced systolic cardiac dysfunction was accompanied by impairment of the SRF–SRE transcriptional complex for cardiomyocyte contractile genes and down-regulation of cardiac actin. Cardiac function as well as the SRF–SRE interaction were improved in the hearts of diabetic mice that had empagliflozin-induced hyperautophagy shutdown and in cardiomyocytes that had empagliflozin-induced inactivation of the autophagy inducer GSK3β, suggesting a key role of high glucose-triggered autophagy in diabetic cardiomyopathy and empagliflozin in reversing it.

In different settings of cardiac disease such as sunitinib-induced cardiac dysfunction[53] or Type 2 diabetic cardiomyopathy,[54] autophagy plays a protective role. Here, EMPA is reported to up-regulate autophagy and ameliorate sunitinib-induced[54] cardiac dysfunction and Type 2 diabetic cardiomyopathy through enhancing cardiomyocyte autophagy via the AMPK/mTOR signalling pathway.[53,54] Furthermore, EMPA ameliorated non-alcoholic fatty liver disease or hepatic steatosis by enhancing hepatic macrophage autophagy via the AMPK/mTOR signalling pathway.[55–57] Comparisons are difficult to make in consideration of the different regulation of autophagy in different disease settings.

Empagliflozin exerts beneficial effects, in the context of heart failure with/without diabetes.[12,13] However, the direct effects of empagliflozin on the heart and cardiac function remain poorly understood. In the present study, the anti-autophagic effect of empagliflozin in response to high glucose was demonstrated. Furthermore, GSK3β may be both a downstream target of empagliflozin and an upstream trigger of the autophagy process. GSK3β has been reported to directly induce autophagy, and in its active state could induce phosphorylation of SRF and its degradation by autophagy in COS-7 cells.[34]

Different effects of EMPA on total GSK3β expression have been reported in Type 2 diabetes-induced cognitive dysfunction.[58] Here, a significant increase in the levels of GSK3β was observed in the high fructose diet-induced hyperglycaemic mice with cognitive disease, which was attenuated by EMPA.[58] Again, in consideration of the subtle and variable regulation of autophagy in different organs and in different settings of disease, any comparison becomes difficult.

Empagliflozin exerts beneficial effects, in the context of heart failure with/without diabetes.[12,13] However, the direct effects of empagliflozin on the heart and cardiac function remain poorly understood. In the present study, the anti-autophagic effect of empagliflozin in response to high glucose was demonstrated. Furthermore, GSK3β may be both a downstream target of empagliflozin and an upstream trigger of the autophagy process. GSK3β has been reported to directly induce autophagy, and in its active state could induce phosphorylation of SRF and its degradation by autophagy in COS-7 cells.[34]

Different effects of EMPA on total GSK3β expression have been reported in Type 2 diabetes-induced cognitive dysfunction.[58] Here, a significant increase in the levels of GSK3β was observed in the high fructose diet-induced hyperglycaemic mice with cognitive disease, which was attenuated by EMPA.[58] Again, in consideration of the subtle and variable regulation of autophagy in different organs and in different settings of disease, any comparison becomes difficult.

A second limitation is the weight loss of mice treated with STZ, which likely was due to the acute onset and progression of diabetes. However, the impact of weight loss on study quality was limited, as we excluded animals with the greatest signs of discomfort. Furthermore, we did not explore the anti-autophagic effects of empagliflozin in rendered diabetic transgenic mice overexpressing GSK3β. Our experiments were not conducted in both sexes, so we do not know which are the possible influences of oestrogenic tone on insulin resistance. Finally, the evidence alone of SGLT2 expression in the total heart is not sufficient to bind all the effects of empagliflozin that we have demonstrated to the receptor. The experiments were not repeated in a knock-out model for SGLT2 (conditional knock-out that has the only down-regulation of SGLT2 in the heart

and not in other tissues, e.g. the kidney), which would allow us to somehow rule out whether the effects of empagliflozin are through the cardiac receptor or are systemic and indirect.

In conclusion, EMPA attenuated LV dysfunction and remodelling in a mouse model of diabetic cardiomyopathy, and the mechanism involved inactivation of the GSK3β pathway, induction of SRF nuclear translocation, and inhibition of GSK3β-mediated hyperactive autophagy (Figure 8) as well as Cx43 laterization. The results of the current study establish a novel role for EMPA in cardiac protection through the autophagy machinery. The interaction between EMPA and the GSK3β pathway is a new therapeutic target for diabetic cardiomyopathy.

References

1. Avogaro A, Vigili de Kreutzenberg S, Negut C, Tiengo A, Scognamiglio R. Diabetic cardiomyopathy: a metabolic perspective. *Am J Cardiol* 2004;93:13A–16A.
2. Okruhlicova L, Tribulova N, Weismann P, Sotnikova R. Ultrastructure and histochemistry of rat myocardial capillary endothelial cells in response to diabetes and hypertension. *Cell Res* 2005;15:532–538.
3. Adameova A, Dhalla NS. Role of microangiopathy in diabetic cardiomyopathy. *Heart Fail Rev* 2014;19:25–33.
4. Takemura G, Miyata S, Kawase Y, Okada H, Maruyama R, Fujiwara H. Autophagic degeneration and death of cardiomyocytes in heart failure. *Autophagy* 2006;2:212–214.
5. Nakai A, Yamaguchi O, Takeda T, Higuchi Y, Hikoso S, Taniike M, Omiya S, Mizote I, Matsumura Y, Asahi M, Nishida K, Hori M, Mizushima N, Otsu K. The role of autophagy in cardiomyocytes in the basal state and in response to hemodynamic stress. *Nat Med* 2007;13:619–624.
6. 6. Yan L, Vatner DE, Kim SJ, Ge H, Masurekar M, Massover WH, Yang G, Matsui Y, Sadoshima J, Vatner SF. Autophagy in chronically ischemic myocardium. *Proc Natl Acad Sci U S A* 2005;102:13807–13812.
7. 7. Shinmura K, Tamaki K, Sano M, Murata M, Yamakawa H, Ishida H, Fukuda K. Impact of long-term caloric restriction on cardiac senescence: caloric restriction ameliorates cardiac diastolic dysfunction associated with aging. *J Mol Cell Cardiol* 2011;50:117–127.
8. 8. Zhang M, Sui W, Xing Y. Angiotensin IV attenuates diabetic cardiomyopathy via suppressing FoxO1-induced excessive autophagy, apoptosis and fibrosis. *Theranostics* 2021;11:8624–8639
9. Dewanjee S, Vallamkondu J, Kalra RS, John A, Reddy PH, Kandimalla R. Autophagy in the diabetic heart: a potential pharmacotherapeutic target in diabetic cardiomyopathy. *Ageing Res Rev* 2021;68:101338.
10. Anker SD, Butler J, Filippatos G. Effect of empagliflozin on cardiovascular and renal outcomes in patients with heart failure by baseline diabetes status: results from the EMPEROR-reduced trial. *Circulation* 2021;143:337–349.
11. Zinman B, Wanner C, Lachin JM, Fitchett D, Bluhmki E, Hantel S, Mattheus M, Devins T, Johansen OE, Woerle HJ, Broedl UC, Inzucchi SE, Empa-Reg Outcome Investigators. Empagliflozin, cardiovascular outcomes, and mortality in type 2 diabetes. *N Engl J Med* 2015;373:2117–2128.
12. Rosenstock J, Marquard J, Laffel LM. Empagliflozin as adjunctive to insulin therapy in type 1 diabetes: the EASE trials. *Diabetes Care* 2018;41:2560–2569.
13. Perkins BA, Soleymanlou N, Rosenstock J. Low-dose empagliflozin as adjunct-to-insulin therapy in type 1 diabetes: a valid modelling and simulation analysis to confirm efficacy. *Diabetes Obes Metab* 2020;22:427–433.
14. Madonna R, Doria V, Minnucci I, Pucci A, Pierdomenico DS, De Caterina R. Empagliflozin reduces the senescence of cardiac stromal cells and improves cardiac function in a murine model of diabetes. *J Cell Mol Med* 2020;24:12331–12340.
15. Kuznetsov AV, Javadov S, Sickinger S, Frotschnig S, Grimm M. H9c2 and HL-1 cells demonstrate distinct features of energy metabolism, mitochondrial function and sensitivity to hypoxia-reoxygenation. *Biochim Biophys Acta* 2015;1853:276–284.

16. Branco AF, Pereira SP, Gonzalez S, Gusev O, Rizvanov AA, Oliveira PJ. Gene expression profiling of H9c2 myoblast differentiation towards a cardiac-like phenotype. *PLoS One* 2015;10:e0129303.
17. Madonna R, Di Napoli P, Massaro M, Grilli A, Felaco M, De Caterina A, Tang D, De Caterina R, Geng YJ. Simvastatin attenuates expression of cytokine-inducible nitric-oxide synthase in embryonic cardiac myoblasts. *J Biol Chem* 2005;280:13503–13511.
18. Moscato S, Cabiati M, Bianchi F. Connexin 26 expression in mammalian cardiomyocytes. *Sci Rep* 2018;8:13975.
19. Madonna R, Pieragostino D, Cufaro MC. Sex-related differential susceptibility to ponatinib cardiotoxicity and differential modulation of the Notch1 signalling pathway in a murine model. *J Cell Mol Med* 2022;26:1380–1391.
20. Madonna R, Moscato S, Polizzi E. Connexin 43 and connexin 26 involvement in the ponatinib-induced cardiomyopathy: sex-related differences in a murine model. *Int J Mol Sci* 2021;22:5815–5835.
21. Madonna R, Pieragostino D, Rossi C. Transplantation of telomerase/myocardin-co-expressing mesenchymal cells in the mouse promotes myocardial revascularization and tissue repair. *Vascul Pharmacol* 2020;135:106807.
22. Neff LS, Bradshaw AD. Cross your heart? Collagen cross-links in cardiac health and disease. *Cell Signal* 2021;79:109889.
23. Tan FH, Putoczki TL, Stylli SS, Luwor RB. Ponatinib: a novel multi-tyrosine kinase inhibitor against human malignancies. *Onco Targets Ther* 2019;12:635–645.
24. Kim S, You D, Jeong Y, Yoon SY, Kim SA, Lee JE. Inhibition of platelet-derived growth factor C and their receptors additionally increases doxorubicin effects in triple-negative breast cancer cells. *Eur J Pharmacol* 2021;895:173868.
25. Madonna R, Giovannelli G, Confalone P, Renna FV, Geng YJ, De Caterina R. High glucose-induced hyperosmolarity contributes to COX-2 expression and angiogenesis: implications for diabetic retinopathy. *Cardiovasc Diabetol* 2016;15:18.
26. Madonna R, Doria V, Gorbe A. Co-expression of glycosylated aquaporin-1 and transcription factor NFAT5 contributes to aortic stiffness in diabetic and atherosclerosis-prone mice. *J Cell Mol Med* 2020;24:2857–2865.
27. Ma H, Guo R, Yu L, Zhang Y, Ren J. Aldehyde dehydrogenase 2 (ALDH2) rescues myocardial ischaemia/reperfusion injury: role of autophagy paradox and toxic aldehyde. *Eur Heart J* 2011;32:1025–1038.
28. Zheng Y, Shi B, Ma M, Wu X, Lin X. The novel relationship between SIRT3 and autophagy in myocardial ischemia-reperfusion. *J Cell Physiol* 2019;234:5488–5495.
29. Wang CY, Chen CC, Lin MH. TLR9 binding to Beclin 1 and mitochondrial SIRT3 by a sodium-glucose co-transporter 2 inhibitor protects the heart from doxorubicin toxicity. *Biology (Basel)* 2020;9:369–397.
30. Tian G, Yu Y, Deng H, Yang L, Shi X, Yu B. Empagliflozin alleviates ethanol-induced cardiomyocyte injury through inhibition of mitochondrial apoptosis via a SIRT1/PTEN/Akt pathway. *Clin Exp Pharmacol Physiol* 2021;48:837–845.
31. Zhang X, Azhar G, Wei JY. SIRT2 gene has a classic SRE element, is a downstream target of serum response factor and is likely activated during serum stimulation. *PLoS One* 2017;12: e0190011.

32. Yang Y, Li Z, Guo J, Xu Y. Deacetylation of MRTF-A by SIRT1 defies senescence induced down-regulation of collagen type I in fibroblast cells. *Biochim Biophys Acta Mol Basis Dis* 2020;1866:165723.
33. Huang S, Shao T, Liu H, Wang Q, Li T, Zhao Q. SIRT6 mediates MRTF-A deacetylation in vascular endothelial cells to antagonize oxLDL-induced ICAM-1 transcription. *Cell Death Discov* 2022;8:96.
34. Luo J, Jin FQ, Yin M, Jin ZG. Regulation of SRF protein stability by an autophagy-dependent pathway. *Biochem Biophys Res Commun* 2020;521:279–284.
35. Hart JR, Vogt PK. Phosphorylation of AKT: a mutational analysis. *Oncotarget* 2011;2:467–476.
36. Zhu X, McAllister D, Lough J. Inhibition of the cardiac alpha-actin gene in embryonic cardiac myocytes by dominant-negative serum response factor. *Anat Rec A Discov Mol Cell Evol Biol* 2003;271:315–321.
37. Madonna R, Geng YJ, Bolli R. Co-activation of nuclear factor-kappaB and myocardin/serum response factor conveys the hypertrophy signal of high insulin levels in cardiac myoblasts. *J Biol Chem* 2014;289:19585–19598.
38. Leybaert L, Lampe PD, Dhein S. Connexins in cardiovascular and neurovascular health and disease: pharmacological implications. *Pharmacol Rev* 2017;69:396–478.
39. Joshi MS, Mihm MJ, Cook AC, Schanbacher BL, Bauer JA. Alterations in connexin 43 during diabetic cardiomyopathy: competition of tyrosine nitration versus phosphorylation. *J Diabetes* 2015;7:250–259.
40. Wang GY, Bi YG, Liu XD. Autophagy was involved in the protective effect of metformin on hyperglycemia-induced cardiomyocyte apoptosis and Connexin43 downregulation in H9c2 cells. *Int J Med Sci* 2017;14:698–704.
41. Iyyathurai J, Decuypere JP, Leybaert L, D'Hondt C, Bultynck G. Connexins: substrates and regulators of autophagy. *BMC Cell Biol* 2016;17(Suppl. 1):20.
42. Falleni A, Moscato S, Sabbatini ARM. Subcellular localization of Connexin 26 in cardiomyocytes and in cardiomyocyte-derived extracellular vesicles. *Molecules* 2021; 26: 6726–6740.
43. Bejarano E, Yuste A, Patel B, Stout RF Jr, Spray DC, Cuervo AM. Connexins modulate autophagosome biogenesis. *Nat Cell Biol* 2014;16:401–414.
44. Mei Y, Thompson MD, Cohen RA, Tong X. Autophagy and oxidative stress in cardiovascular diseases. *Biochim Biophys Acta* 2015;1852:243–251.
45. Ren J, Taegtmeyer H. Too much or not enough of a good thing—the Janus faces of autophagy in cardiac fuel and protein homeostasis. *J Mol Cell Cardiol* 2015;84:223–226.
46. He C, Zhu H, Li H, Zou MH, Xie Z. Dissociation of Bcl-2-Beclin1 complex by activated AMPK enhances cardiac autophagy and protects against cardiomyocyte apoptosis in diabetes. *Diabetes* 2013;62:1270–1281.
47. Tong M, Saito T, Zhai P. Mitophagy is essential for maintaining cardiac function during high fat diet-induced diabetic cardiomyopathy. *Circ Res* 2019;124:1360–1371.
48. Yao Q, Ke ZQ, Guo S. Curcumin protects against diabetic cardiomyopathy by promoting autophagy and alleviating apoptosis. *J Mol Cell Cardiol* 2018;124:26–34.

49. Mellor KM, Varma U, Stapleton DI, Delbridge LM. Cardiomyocyte glycophagy is regulated by insulin and exposure to high extracellular glucose. *Am J Physiol Heart Circ Physiol* 2014;306:H1240–H1245.
50. Zhao L, Zhang Q, Liang J, Li J, Tan X, Tang N. Astrocyte elevated gene-1 induces autophagy in diabetic cardiomyopathy through upregulation of KLF4. *J Cell Biochem* 2019;120:9709–9715.
51. Kanamori H, Takemura G, Goto K. Autophagic adaptations in diabetic cardiomyopathy differ between type 1 and type 2 diabetes. *Autophagy* 2015;11:1146–1160.
52. De Meyer GR, De Keulenaer GW, Martinet W. Role of autophagy in heart failure associated with aging. *Heart Fail Rev* 2010;15:423–430.
53. Ren C, Sun K, Zhang Y. Sodium-glucose cotransporter-2 inhibitor empagliflozin ameliorates sunitinib-induced cardiac dysfunction via regulation of AMPK-mTOR signaling pathway-mediated autophagy. *Front Pharmacol* 2021;12:664181.
54. Aragon-Herrera A, Feijoo-Bandin S, Otero Santiago M. Empagliflozin reduces the levels of CD36 and cardiotoxic lipids while improving autophagy in the hearts of Zucker diabetic fatty rats. *Biochem Pharmacol* 2019;170:113677.
55. Meng Z, Liu X, Li T. The SGLT2 inhibitor empagliflozin negatively regulates IL-17/IL-23 axis-mediated inflammatory responses in T2DM with NAFLD via the AMPK/mTOR/autophagy pathway. *Int Immunopharmacol* 2021;94:107492.
56. Nasiri-Ansari N, Nikolopoulou C, Papoutsi K. Empagliflozin attenuates non-alcoholic fatty liver disease (NAFLD) in high fat diet fed ApoE((-/-)) mice by activating autophagy and reducing ER stress and apoptosis. *Int J Mol Sci* 2021;22:9709–9715.
57. Li T, Fang T, Xu L. Empagliflozin alleviates hepatic steatosis by activating the AMPK-TET2-autophagy pathway in vivo and in vitro. *Front Pharmacol* 2020;11:622153.
58. Khan T, Khan S, Akhtar M, Ali J, Najmi AK. Empagliflozin nanoparticles attenuates type 2 diabetes induced cognitive impairment via oxidative stress and inflammatory pathway in high fructose diet induced hyperglycemic mice. *Neurochem Int* 2021;150:105158.
59. Schliess F, von Dahl S, Haussinger D. Insulin resistance induced by loop diuretics and hyperosmolarity in perfused rat liver. *Biol Chem* 2001;382:1063–1069.
60. Waldhausl W, Kleinberger G, Korn A, Dudczak R, Bratusch-Marrain P, Nowotny P. Severe hyperglycemia: effects of rehydration on endocrine derangements and blood glucose concentration. *Diabetes* 1979;28:577–584.
61. Lupsa BC, Inzucchi SE. Diabetic Ketoacidosis and Hyperosmolar Hyperglycemic Syndrome. Totowa, NJ: Humana Press; 2014.
62. Bratusch-Marrain PR, DeFronzo RA. Impairment of insulin-mediated glucose metabolism by hyperosmolality in man. *Diabetes* 1983;32:1028–1034.
63. Madonna R, Pieragostino D, Rossi C. Simulated hyperglycemia impairs insulin signaling in endothelial cells through a hyperosmolar mechanism. *Vascul Pharmacol* 2020;130:106678.

Figures

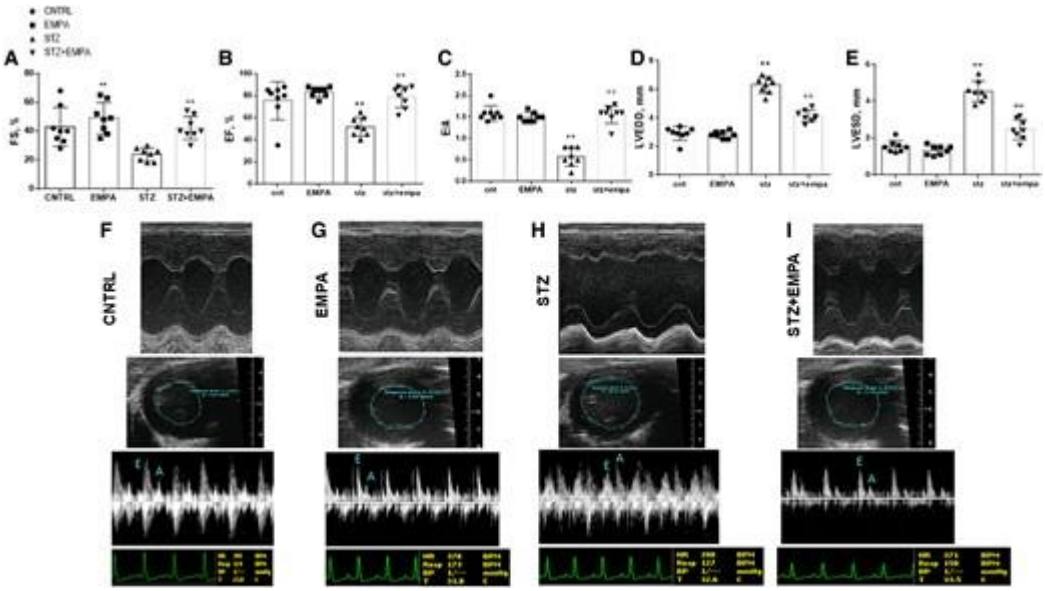

Figure 1. Effects of streptozotocin and empagliflozin on cardiac function in mice. (A) Fractional shortening (FS), (B) Ejection fraction (EF), (C) E/A ratio, (D) LV end-diastolic diameter, and (E) LV end-systolic diameter measured by echocardiography in the different treatment groups such as CNTRL (saline vehicle), EMPA, STZ, and STZ + EMPA. (F–I), Representative M-mode images in parasternal long-axis view, B-mode images in parasternal short-axis view, recordings of mitral valve inflow by pulsed wave Doppler in apical four-chamber view, and electrocardiogram traces among different groups. Data are expressed as means ± standard deviations (SDs) (one-way ANOVA, Tukey HSD post hoc test, n = 8 mice per treatment group). **P < 0.01 vs. CNTRL (saline vehicle); °°P < 0.01 vs. STZ. CNTRL, control; EMPA, empagliflozin; STZ, streptozotocin.

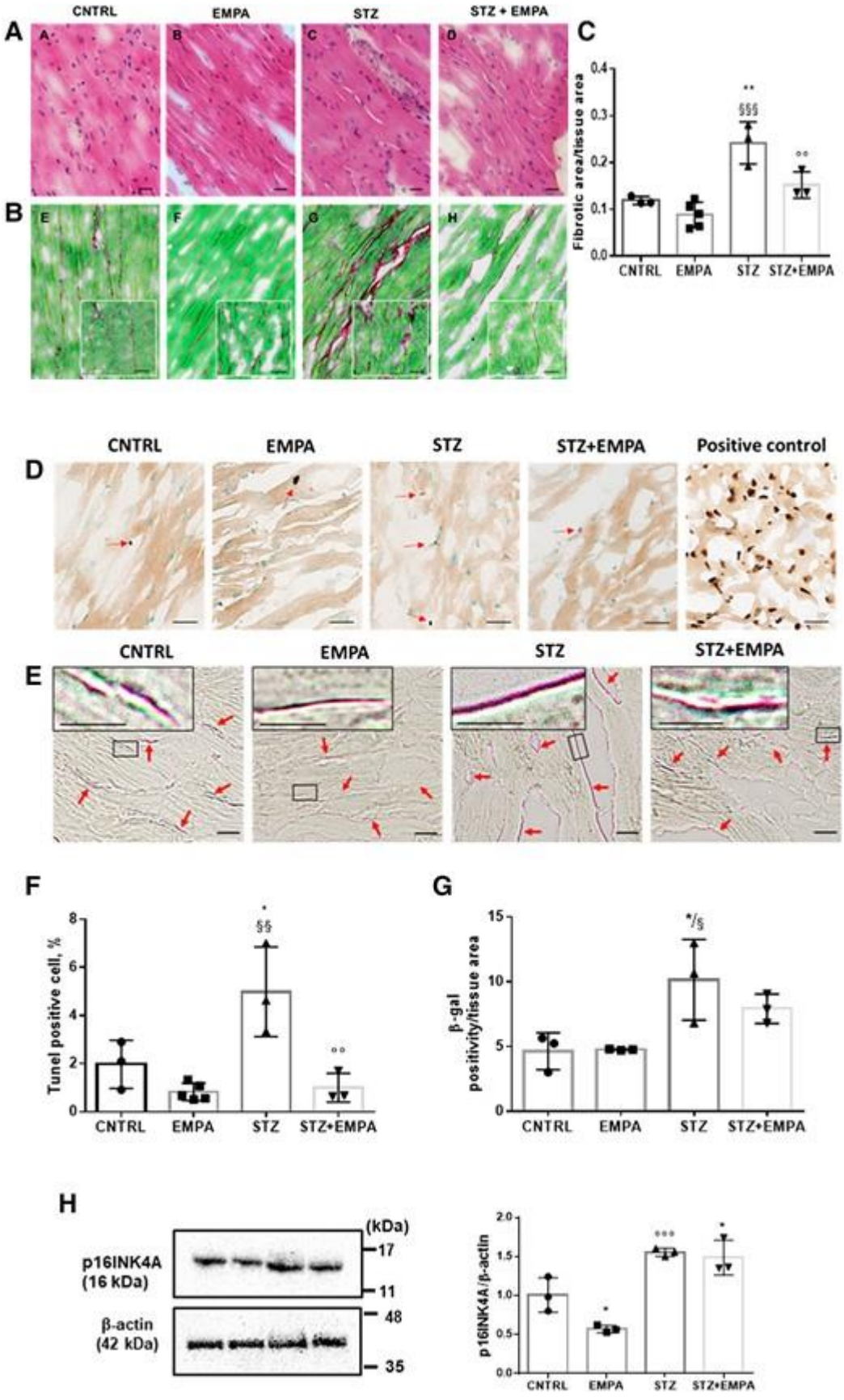

Figure 2. Empagliflozin exerts anti-fibrotic, anti-apoptotic, and anti-senescent effects in diabetic hearts. (A–C) Heart morphology and fibrosis. (A) Haematoxylin–eosin staining. Scale bar 20 µm.

Original magnification ×400. (B) Sirius red staining. Representative images from murine heart sections. Scale bar 20 µm. Original magnification ×400. (C) Image analysis data of fibrosis staining are expressed as mean of fibrosis area/tissue area ± SD; **P < 0.01 vs. CNTRL (saline vehicle); §§§P < 0.001 vs. EMPA; °P < 0.05 vs. STZ. (D–G) Heart apoptosis and senescence. (D) Representative images of TUNEL assay on murine heart sections. Arrows indicate apoptotic nuclei. Scale bar 20 µm. Original magnification ×400. (E) Representative images of β-gal expression from murine heart sections. Arrows indicate β-galactosidase deposits. Scale bar 10 µm. Original magnification ×1000. Inserts are a magnification of the squared areas. (F) Quantification of TUNEL-positive cells is reported as the mean percentage of TUNEL-positive cells on total cell number (ranging between 600 and 2000) ± SD; *P < 0.05 vs. CNTRL; §§P < 0.01 vs. EMPA; °°P < 0.01 vs. STZ. (G) Image analysis data of β-gal expression are expressed as mean of β-gal positivity/tissue area ± SD, *P < 0.05 vs. CNTRL; §P < 0.05 vs. EMPA. Each experiment was repeated three times, on n = 3 mice and on three non-consecutive slices of tissue for each mouse. Statistical analysis was done by one-way ANOVA test and Tukey HSD post hoc test. (H) Western blots for p16INK4A. Representative western blots of p16INK4A. Densitometric analysis of western blot was normalized to β-actin and used as internal control. Results are reported as mean ± SD of n = 3 mice, and each experiment was repeated at least three times. Statistical analysis was done by one-way ANOVA test and Tukey HSD post hoc test. *P < 0.05 vs. CNTRL; °°°P < 0.001 vs. EMPA.

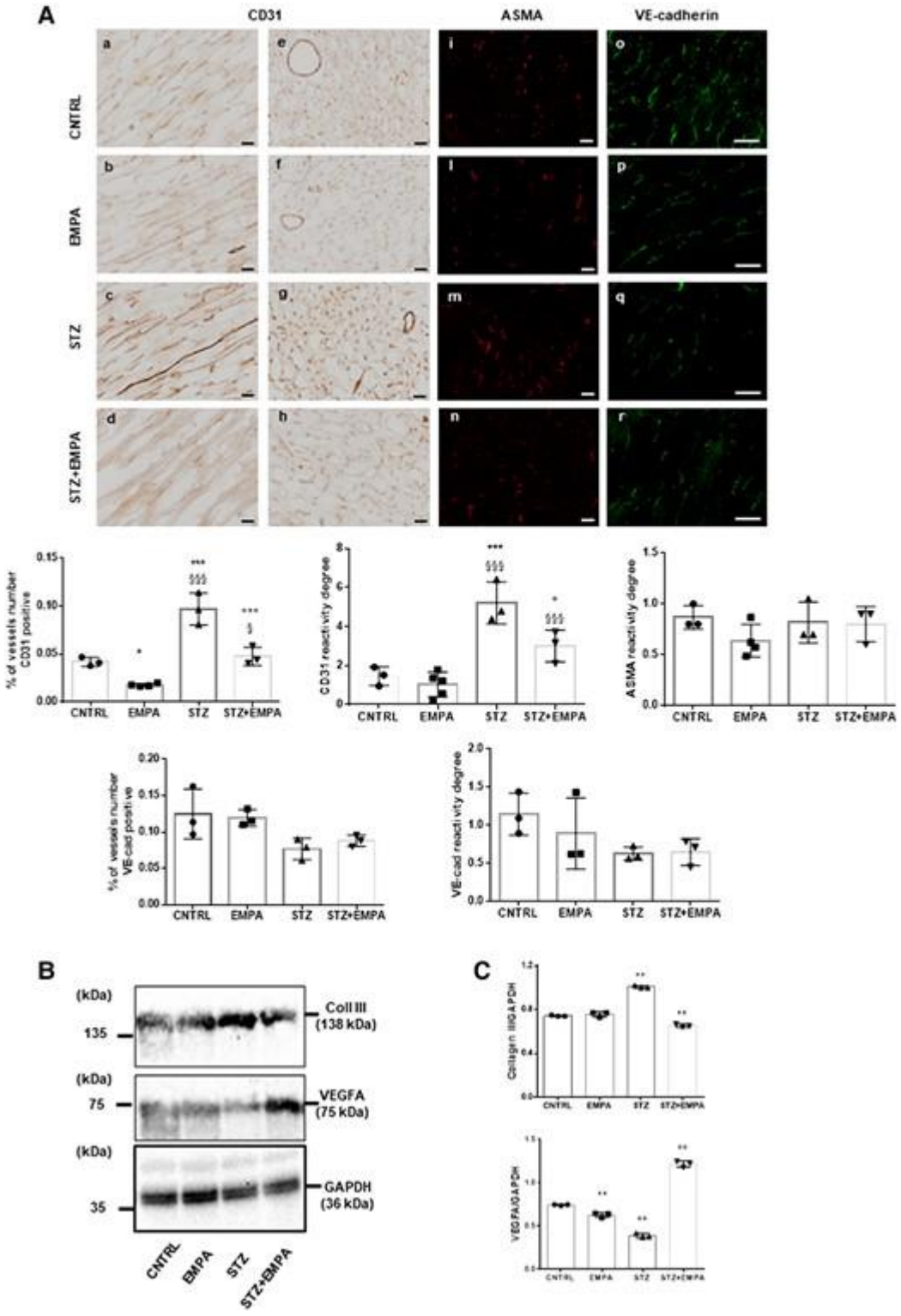

Figure 3. Empagliflozin exerts anti-angiogenic and anti-remodelling effect in diabetic and control hearts. (A) CD31, ASMA, and VE-cadherin immunoreactivity. Representative images of CD31 (a–d longitudinal section, e–h cross-section; scale bar 20 µm, original magnification ×400), ASMA (i–n; scale bar 100 µm, original magnification ×4), and VE-cadherin (o–r; scale bar 20 µm, original magnification ×400) expression on murine heart sections. The graphs represent the quantification of CD31 and VE-cadherin-positive vessels and of CD31, ASMA, and VE-cadherin immunoreactivity. The percentage of vessel number, mean ± SD, has been obtained as described in Section 2; *P <

0.05, ***P < 0.001 vs. CNTRL (saline vehicle); §P < 0.05, §§§P < 0.001 vs. EMPA; °°°P < 0.001 vs. STZ. Data of CD31, ASMA, and VE-cadherin reactivity are expressed as the mean of CD31 or ASMA or VE-cadherin-positive area/tissue area ± SD; ***P < 0.001 vs. CNTRL; §P < 0.05, §§§P < 0.001 vs. EMPA; °P < 0.05 vs. STZ. Each experiment was repeated three times, on n = 3 mice and on three non-consecutive slices of tissue for each mouse. Statistical analysis was done by one-way ANOVA test and Tukey HSD post hoc test. (B) Western blots for Collagen III and VEGFA. Representative western blots of Collagen III. (C) Western blot for VEGFA. Representative western blots of VEGFA. Densitometric analysis of (B and C) western blot was normalized to GAPDH and used as internal control. Results are reported as mean ± SD of n = 5 mice, and each experiment was repeated at least three times. Statistical analysis was done by one-way ANOVA test and Tukey HSD post hoc test. *P < 0.05, **P < 0.01 vs. CNTRL; °°P < 0.01 vs. STZ.

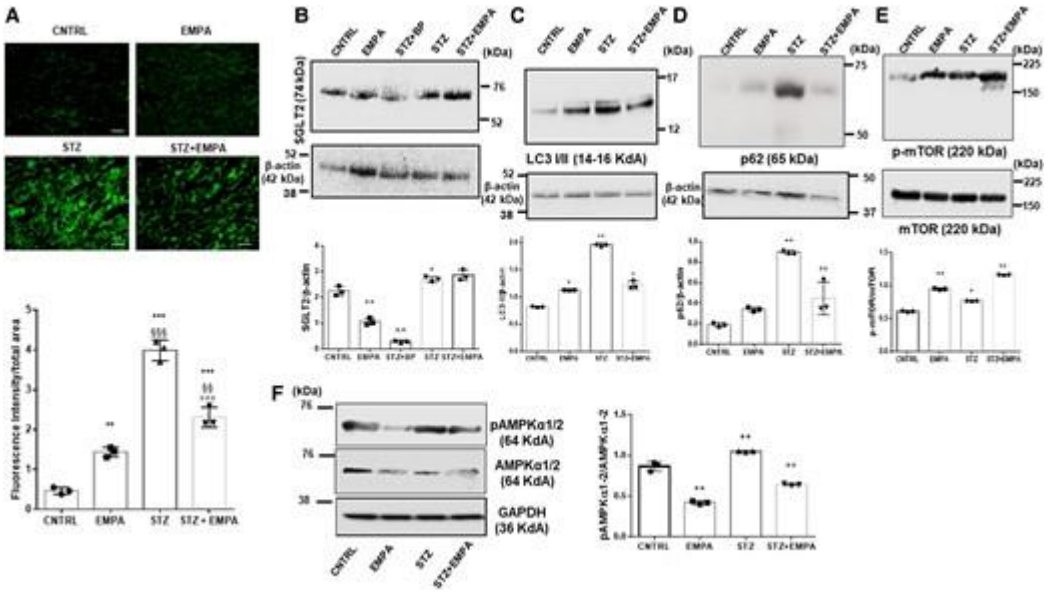

Figure 4. Empagliflozin alleviates excessive autophagy in diabetic hearts. (A) Heart tissue autophagy. Representative confocal microscopy images of green detection reagent indicating the presence of autophagic vacuoles. Scale bar 100 µm. Original magnification ×10. The graph represents image analysis of fluorescence reported as means ± SD; **P < 0.01, ***P < 0.001 vs. CNTRL (saline vehicle); §§P < 0.01, §§§P < 0.001 vs. EMPA; °°°P < 0.001 vs. STZ. Each experiment was repeated three times, on n = 3 mice and on three non-consecutive slices of tissue for each mouse. Statistical analysis was done by one-way ANOVA test and Tukey HSD post hoc of n = (n = 3 mice, each experiment repeated at least three times). (B–F) Western blots and densitometry for SGLT2 (B) and autophagy markers such as LC3 (C), p62 (D), p-mTOR (E), pAMPK1/2 (F) on heart tissue lysates. GAPDH or β-actin was used as internal control. Results are reported as mean ± SD of n = 5 mice, and each experiment was repeated at least three times. Statistical analysis was done by one-way ANOVA test and Tukey HSD post hoc test. *P < 0.05, **P < 0.01 vs. CNTRL; °P < 0.05, °°P < 0.01 vs. STZ, ^^P < 0.01 vs. all treatment groups.

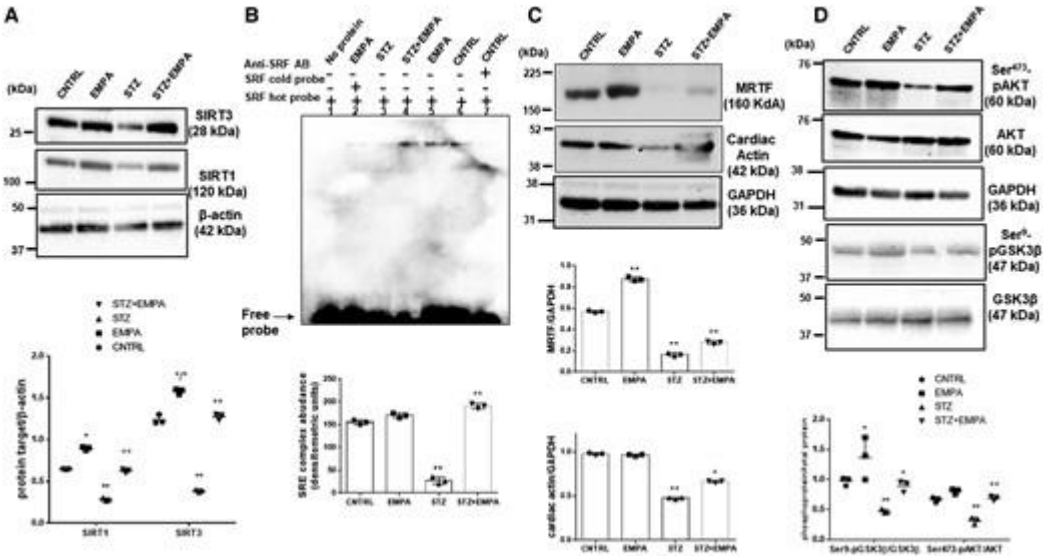

Figure 5. Empagliflozin induces sirtuins, activates PI3/AKT and SRF–SRE, and inhibits GSK3β in diabetic and control hearts. (A) Western blots of SIRT1 and SIRT3. Representative images of western blot analysis of SIRT1 and SIRT3 in heart tissue lysates. (B) EMSA assessing the SRF–SRE binding activity in cardiac nuclear proteins. The specificity of the SRF–SRE complex formation was determined by competition with both unlabelled oligonucleotides (cold SRF probe) and by the presence of a supershift after the addition of an anti-SRF antibody. Here shown is a representative EMSA from three independent experiments. Densitometry of protein–DNA complexes in three different EMSA experiments. (C) Western blot of myogenic transcription factors and sarcomeric proteins. Representative images of western blot and related densitometric analysis of myocardin-related transcription factor (MRTF) and cardiac actin in heart tissue lysates. (D) Western blots for pAKT, AKT, and pGSK3β. Representative images of western blot analysis of pAKT, AKT, and pGSK3β in heart tissue lysates and related densitometric analysis. GAPDH or β-actin was used as internal control. Results are reported as mean ± SD (n = 5 mice, each experiment repeated at least three times). Statistical analysis was done by two-way ANOVA test and Tukey HSD post hoc test. *P < 0.05, **P < 0.01 vs. CNTRL; °P < 0.05, °°P < 0.01 vs. STZ.

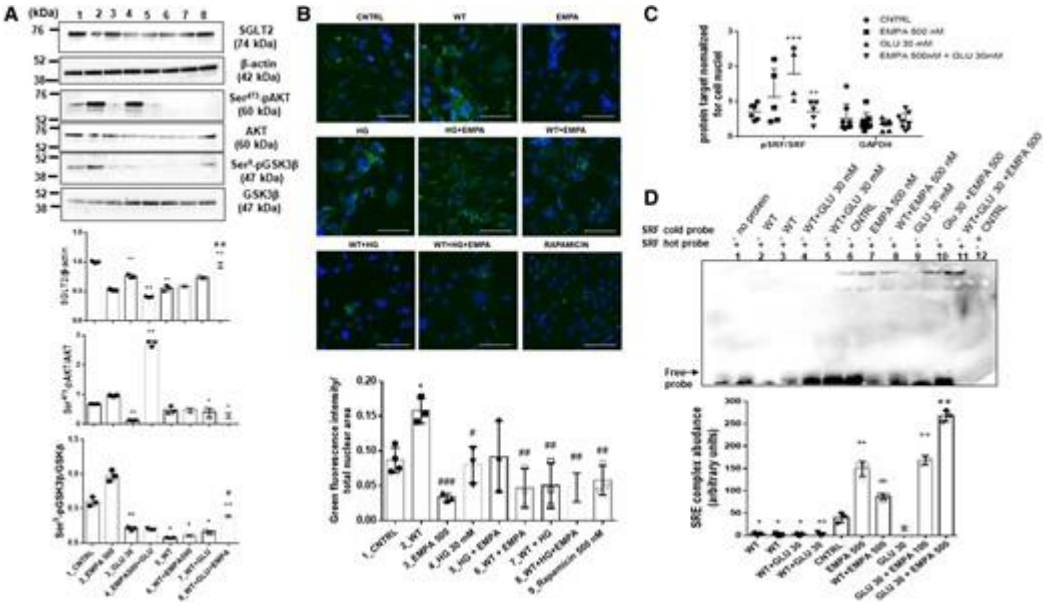

Figure 6. Empagliflozin inhibits autophagy through AKT/GSK3β signalling pathway, decreases SRF phosphorylation, and reactivates the cardiomyogenic transcriptional complex SRF–SRE in cardiomyocytes chronically exposed to high glucose. (A) Western blot for SGLT2 and AKT/GSK3β signalling. Representative western blots for SGLT2, pAKT, AKT, pGSK3β, pGSK3β, and related densitometric analysis in cardiomyocyte lysates. β-Actin was used as internal control. Results are reported as mean ± SD of three different gels (n = 3 independent experiments). Statistical analysis was done by one-way ANOVA test and Tukey HSD post hoc test. *P < 0.05, **P < 0.01 vs. CNTRL; °P < 0.05, °°P < 0.01 vs. Glu 30 mM; ^P < 0.05 vs. WT; #P < 0.05, ##P < 0.01 vs. Glu 30 mM + WT. (B) Cardiomyocyte autophagy. Representative images of autophagic cardiomyocytes after different treatments (a–i). Scale bar 50 µm. The graph represents the image analysis of fluorescent autophagic vacuoles. Data are reported as the mean of green fluorescence intensity/total nuclear area ± SD of n = 3 wells for each treatment. Statistical analysis was done by one-way ANOVA and Tukey HSD post hoc test. *P < 0.05, **P < 0.01 vs. CNTRL; #P < 0.05, ##P < 0.01 vs. WT. (C) ELISA assessing the SRF phosphorylation in cardiomyocytes. Results were expressed as a ration between pSRF normalized for cell nuclei/SRF normalized for cell nuclei or GAPDH normalized for cell nuclei, and reported as mean ± SD of three replicates for each treatment (n = 3 independent experiments). Statistical analysis was done by one-way ANOVA test and Tukey HSD post hoc test. ***P < 0.001 vs. CNTRL; °°P < 0.05 vs. Glu 30 mM. (D) EMSA assessing the SRF–SRE binding activity in cardiomyocyte nuclear proteins. The specificity of the SRF–SRE complex formation was determined by competition with unlabelled oligonucleotides (cold SRF probe). Here shown is a representative EMSA from three independent experiments. Densitometry of protein–DNA complexes in three different EMSA experiments. Statistical analysis was done by one-way ANOVA and Tukey HSD post hoc test. *P < 0.05, **P < 0.01 vs. CNTRL; °P < 0.05, °°P < 0.01 vs. Glu 30 mM; ^P < 0.05, ^^P < 0.01 vs. WT; #P < 0.05, ##P < 0.01 vs. Glu 30 mM + WT.

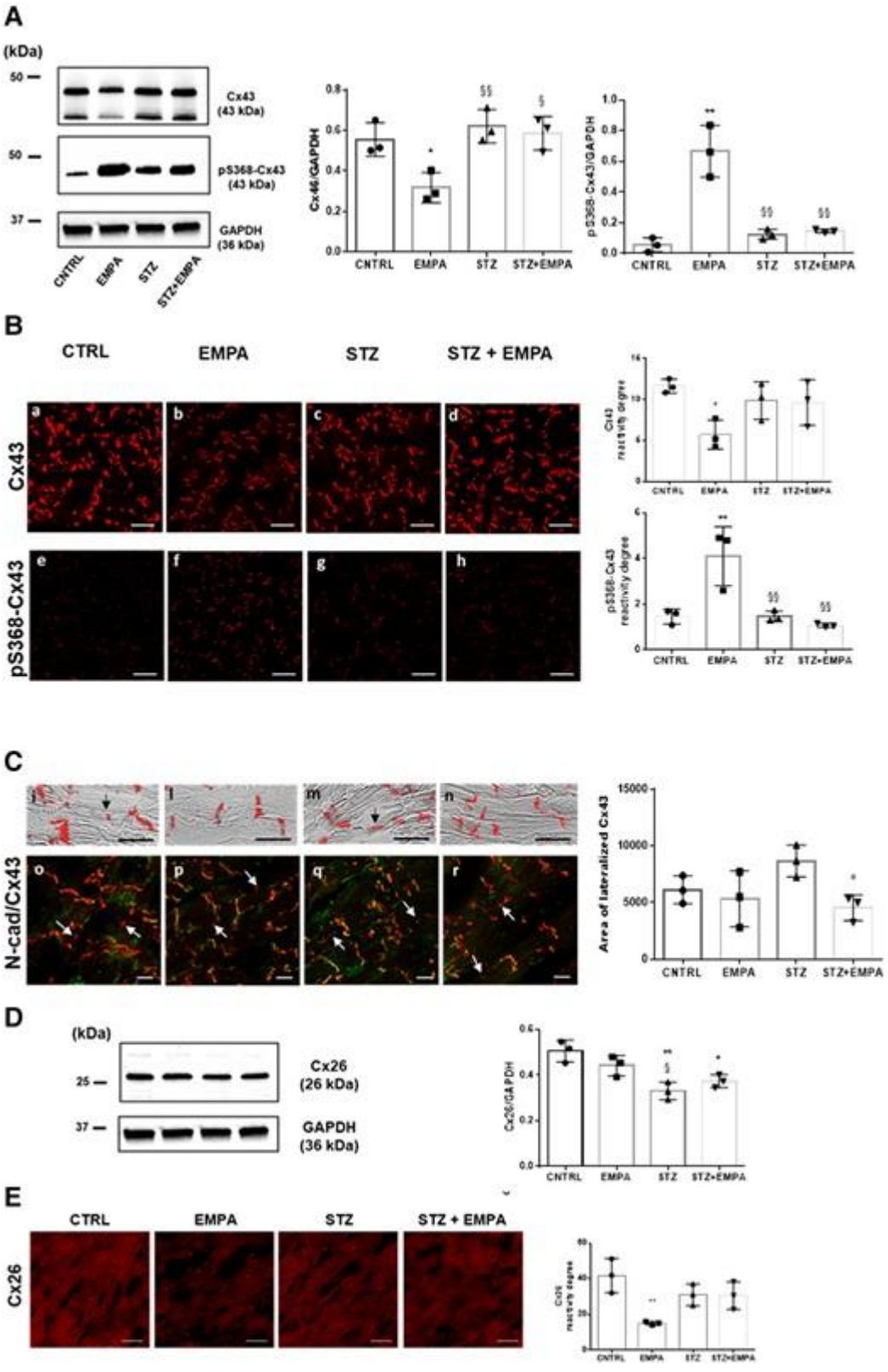

Figure 7. Cardiac connexin expression. (A) Heart tissue Cx43. Representative western blots of Cx43 and pS368-Cx43 in heart tissue lysates and quantification. Densitometric analysis was normalized to GAPDH and used as internal control. Results are reported as mean ± SD of three different gels (n = 3). *P < 0.05, **P < 0.01, vs. CNTRL; §P < 0.05, §§P < 0.01 vs. EMPA. (B) Cardiomyocytes Cx43. Representative images of Cx43 (a–d) and pS368-Cx43 (e–h)

immunofluorescence on ventricle hearts from control or treated mice. Scale bar 50 µm. Original magnification ×200. Relative image analysis of Cx43 and pS368-Cx43 immunofluorescence are shown on the right side; *P < 0.05, **P < 0.01 vs. CTRL; §§P < 0.01 vs. EMPA. (C) Cx43 lateralization. (i–n) Confocal laser scanning microscopy: representative three-dimensional images of the maximum intensity projection of mice cardiomyocyte longitudinal sections. Cx43 (red) is mainly expressed in the intercalated discs, whereas in CNTRL and STZ-treated mice, it is also present along the lateral border (arrow). Scale bar 20 µm. Original magnification ×400. (o–r) Representative images of Cx43 (red) and N-cadherin (green) double immunofluorescence. Yellow corresponds to red and green colocalization. Arrows point Cx43 present on lateral margins of cardiomyocytes in different experimental conditions. Scale bar 20 µm. Original magnification ×400. Image analysis of lateral Cx43 immunofluorescence is shown on the lateral side; °P < 0.05 vs. STZ. (D) Heart tissue Cx26. Representative western blots of connexin Cx26 and quantification. Densitometric analysis was normalized to GAPDH and used as internal control. Results are reported as mean ± SD of three different gels (n = 3). *P < 0.05, **P < 0.01 vs. CNTRL; §P < 0.05 vs. EMPA. (E) Cardiomyocytes Cx26. Representative images of Cx26 immunofluorescence on ventricle hearts from control or treated mice. Scale bar 50 µm. Original magnification ×200. Relative image analysis of Cx26 immunofluorescence is shown on the right side; *P < 0.05 vs. CNTRL. Each experiment was repeated three times, on n = 3 mice and on three non-consecutive slices of tissue for each mouse.

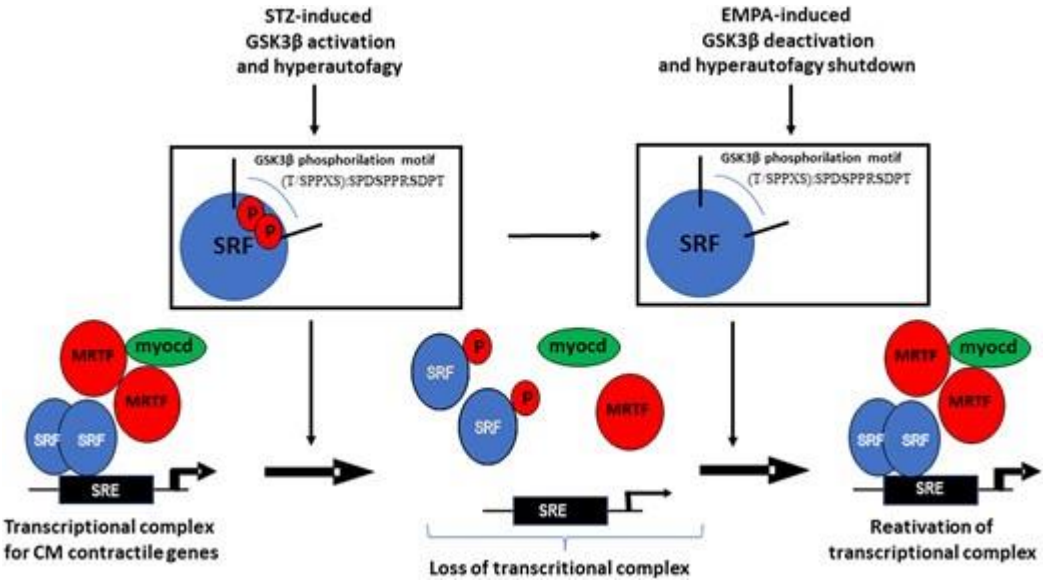

Figure 8. Schematic representation of SRF–SRE interaction in mice exposed to streptozotocin and empagliflozin. MYOCD, SRF, and MRTF maintain cardiomyocyte contractile gene expression. In conditions of STZ-induced diabetes, GSK3β is activated, induces autophagy, and degrades SRF through GSK3β phosphorylation motif (T/SPPXS):SPD**S**PPR**S**DPT. This leads to the loss of SRF–SRE interactions at cardiomyocyte promoters. EMPA inhibits excessive autophagy by inhibiting GSK3β, leading to reactivation of the cardiomyocyte transcriptional complex. Abbreviations: MYOCD, myocardin; SRF, serum response factor; MRTF, myocardin-related transcription factor; SRE, serum response element; STZ, streptozotocin; GSK3β, glycogen synthase kinase 3 beta.